Available online at www.sciencedirect.com
SCIENCE DIRECT®
International Journal of Heat and Mass Transfer 48 (2005) 1480–1493
International Journal of HEAT and MASS TRANSFER
www.elsevier.com/locate/ijhmt

Impact of leading edge delta-wing vortex generators on the thermal performance of a flat tube, louvered-fin compact heat exchanger

A. Joardar, A.M. Jacobi *

Department of Mechanical and Industrial Engineering, University of Illinois, 1206 West Green Street, Urbana-Champaign, IL 61801, United States

Received 9 June 2004; received in revised form 18 October 2004
Available online 13 December 2004

Abstract

The effectiveness of delta-wing type vortex generators is experimentally evaluated by full-scale wind-tunnel testing of a compact heat exchanger typical to those used in automotive systems. The mechanisms important to vortex enhancement methods are discussed, and a basis for selecting a delta-wing design as a vortex generator is established. The heat transfer and pressure drop performance are assessed at full scale under both dry- and wet-surface conditions for a louvered-fin baseline and for a vortex-enhanced louvered-fin heat exchanger. An average heat transfer increase over the baseline case of 21% for dry conditions and 23.4% for wet conditions was achieved with a pressure drop penalty smaller than 7%. Vortex generation is proven to provide an improved thermal-hydraulic performance in compact heat exchangers for automotive systems.

1. Introduction

Plate-and-fin compact heat exchangers with multi-louver fins are currently used in automotive air conditioning for passenger comfort. Increasing demands are being placed on heat exchanger performance for reasons of compactness, economy in manufacturing and operating costs, energy conservation and even for ecological reasons. The importance of these issues continues to motivate the study of enhancement techniques. In a typical refrigerant-to-air heat exchanger, the air-side convective resistance to heat transfer is dominant, at 75% or more of the total thermal resistance. Therefore, many techniques for enhancing heat transfer focus on the air-side surface.

Enhancement of air-side heat transfer using passive vortex generators is a promising technique in a range of applications. In this method, protuberances such as delta-wings are used to generate streamwise vortices that are carried through the heat exchanger by the main flow and induce bulk fluid mixing and a reduced thickness of the thermal boundary layer. This enhancement method has the important advantage of low cost and ease of implementation, with a usually modest pressure drop penalty. However, strategies for vortex-generator design and appropriate placement have not been described in the open literature for highly compact heat exchangers which are essential to fully exploit the method.

* Corresponding author. Present address: 140 Mechanical Engineering Building, MC-244, 1206 West Green Street, Urbana, IL 61801, United States. Tel.: +1 217 333 4108; fax: +1 217 244 6534.
E-mail address: a-jacobi@uiuc.edu (A.M. Jacobi).

0017-9310/$ - see front matter © 2004 Elsevier Ltd. All rights reserved.
doi:10.1016/j.ijheatmasstransfer.2004.10.018

Nomenclature

A	surface area, m^2
b	span of delta wing, m (Fig. 1(a))
b_s	see Eq. (30), kg_w/kg_a °C
c	delta wing chord length, m (Fig. 1(a))
C	heat rate capacity = $\dot{m}c_p$, kW/K
C_r	heat capacity ratio = C_{min}/C_{max}, dimensionless
c_p	specific heat at constant pressure, kJ/kg K
D_h	hydraulic diameter = $4A_{min}L/A_T$, m
E	fan power per unit core volume, kW/m^3
f	friction factor, see Eq. (19), dimensionless
$2F_h$	fin height between the tubes, m (Fig. 4)
F_p	fin pitch, m
G	mass flux of air based on minimum flow area = ρV_{max}, kg/m^2 s
h	convection heat transfer coefficient, kW/m^2 K
i	specific enthalpy, kJ/kg
j	colburn j-factor = $Nu/(Re \cdot Pr^{1/3})$, dimensionless
k	thermal conductivity, kW/m^2 K
L_{core}	effective flow length from inlet to exit of exchanger, mm
Le	Lewis number = Sc/Pr, dimensionless
$\dot{m}$	mass flow rate, kg/s
n	number of passes per partition
N	number of fins, dimensionless
Nu	Nusselt number = $h \cdot D_h/k$, dimensionless
ΔP_{core}	air side pressure drop across exchanger, Pa
Pr	Prandtl number, dimensionless
q	heat transfer rate, kW
R	thermal resistance, K/kW
Re	Reynolds number, dimensionless
Sc	Schimdt number, dimensionless
t_f	fin thickness, m
T	temperature, K
U	overall heat transfer coefficient, kW/m^2 K
V	velocity, m/s
Z	see Eq. (22), kW/m^3 K
α	wing angle of attack
β	$4\sigma/D_h$, m^2/m^3
ε	heat exchanger effectiveness = Q_{avg}/Q_{max}, dimensionless
η	fin efficiency, see Eq. (16), dimensionless
μ	dynamic viscosity of fluid, kg/m s
θ	louver angle (Fig. 4)
ξ	see Eq. (28), dimensionless
ρ	mass density of fluid, kg/m^3
σ	area ratio = A_{min}/A_{fr}, dimensionless
ω	humidity ratio = kg_w/kg_a, dimensionless
Λ	wing aspect ratio = $2b/c$, dimensionless (Fig. 1(a))

Subscripts

a	air
c	coolant or refrigerant side
d	dry condition
f	fin
i	inlet to partition/exchanger
int	intermediate between partitions
m	mean value
o	outlet of partition/exchanger
p	pass
s	saturated condition
T	total
w	tube wall
1, 2	first and second partition respectively

Considerable research has been directed at vortex-enhanced heat transfer for different generators, surface geometries, and flow conditions [1–5]. However, due to the complexity of the underlying phenomena, most studies have employed highly idealized geometries and flow conditions. Although much of the work in vortex generators has been aimed at their potential application in heat exchangers, their effectiveness has not been assessed adequately in full-scale heat exchangers.

1.1. Background

In order to understand the thermo-fluid mechanisms important to vortex-enhanced heat transfer, most early research considered flows between flat plates. Edwards and Alker [6] investigated the effectiveness of cubes and delta winglets for heat transfer enhancement. They found winglet vortices persisting over greater flow lengths as compared to those generated by a cube. The winglet generators resulted in a higher overall enhancement; however, cubes produced greater local enhancements. A counter-rotating vortex pair, such as that produced by a wing, was more effective than a similar co-rotating pair. In the experiments of Katoaka et al. [7] it was shown that the enhancement in the region between two neighboring counter-rotating vortices was achieved only on the side where the imposed flow was toward the surface and not away from it. Since surface directed stagnation flow causes boundary layer thinning, these results suggest that heat transfer enhancement could be attributed to modification of thermal boundary layer. Torii et al. [8] measured the local heat transfer downstream of a delta-wing on a flat plate. Using the naphthalene sublimation technique they reported

enhancements over 200% in the downwash region. Gentry and Jacobi [9] studied interactions between longitudinal vortices from delta wing and the laminar boundary layer on a flat plate. For a Reynolds number range of 600–1000 based on plate length, they reported average heat transfer enhancements of 50–60%. In 1993, Yanagihara and Torii [10] extended their earlier work investigating the effects of multiple arrays of winglet vortex generators on the local and average heat transfer of a laminar boundary layer. They studied both co-rotating and counter-rotating longitudinal vortices and achieved best results with counter-rotating vortices.

Vortex-enhanced channel flows have received considerable attention, because of their importance to heat exchanger geometries. The two different types of vortex generators that have been studied in detail are delta and rectangular wings, and winglet pairs placed either stand alone or in rows. A wing or winglet can be constructed as a separate piece and mounted on the channel or can be stamped out of fin stock with only the cord attached, leaving a hole in the channel floor. For wing-type vortex generators, the most important geometric parameters are angle of attack, aspect ratio and an appropriate ratio of vortex generator area to heat transfer area. In general, according to Fiebig [2,3], delta wings are more effective than rectangular wings, and punched wings are marginally better than mounted wings for identical vortex generator area. Heat transfer and pressure drop increase with angle of attack up to a certain maximum when significant changes in vortex structure occur, in particular transition from longitudinal to more transverse vortices takes place; the latter dominate at 90° angle of attack. These issues gain significance in design of delta wings for a specific application.

Fiebig and co-workers [11] systematically compared delta and rectangular wings and winglets using unsteady liquid-crystal thermography. In their study, the reference fin area varied from 60 times the wing area for the delta wing, to 38 for the delta winglet pair, to 30 for the rectangular wing and 19 for rectangular winglet pair. They considered vortex-generator aspect ratios from 0.8 to 2.0 and attack angles from 10° to 60° over Reynolds numbers (based on plate spacing) from 1000 to 2000. Local heat transfer enhancements of up to 200% were reported with a 60% increase in drag coefficient. They concluded that the delta-wing vortex generator provided the largest enhancement of those studied. Gentry and Jacobi [12] used naphthalene sublimation to measure the performance of vortex generators. They reported average enhancements of 20–50% with accompanying pressure drop penalty of 50–110%, for Reynolds numbers ranging from 400–2000. Ge et al. [13] systematically investigated the impact of multiple vortex generators on offset-strip fin arrays using PIV and naphthalene sublimation techniques. They reported a maximum enhancement of 32% at $Re = 1000$ for two rows of delta-wings, one at the array inlet and one at half the flow length. Computational studies support these favorable assessments of the thermal-hydraulic performance of vortex generators in channel flows and complex geometries. Biswas and Chattopadhyay [14] predicted a 34% increase in spanwise average Nusselt number with a 79% increase in friction factor for a built-in delta-wing with $\alpha = 26$, $\Lambda = 1.0$ and ratio of wing span to channel width being 0.375. The corresponding heat transfer and friction factor results for stamped wing were lower. Brockmeier et al. [15] compared their numerical results for delta wings in a channel flow (fully developed) to experimental data for other high-performance surfaces. They found the performance of vortex generators to be superior to that of plain-fin, offset strip and louvered-fin geometries.

Channels with tubes have also been studied to better simulate heat exchanger geometries. Fiebig et al. [16] considered heat exchanger elements with 3 tube rows and a delta-winglet pair downstream of each tube. For an inline tube arrangement they measured a 55–65% increase in heat transfer, with a pressure drop increase of 20–45%. The staggered arrangement resulted in less enhancement and pressure loss. Numerical studies have also addressed vortex generators in channel flows with tubes. In 1994 Biswas et al. [17] reported that a delta-winglet pair downstream of tube results in up to 240% local enhancement of the heat transfer in the recirculation zone. For punched delta-winglets in such a flow configuration, the numerical predictions of Fiebig et al. [18] showed a 31% enhancement at $Re = 300$. In 1999, Jahromi et al. [19] reported 20–50% enhancements with similar configuration for a Re range of 400–1200. The ratio of increase in Nusselt number to the increase in friction factor ranged between 0.65 and 0.78.

Other studies have focused on the effectiveness of vortex generators applied to prototype heat exchangers. In an early report, Russel et al. [20] used the transient-melt-line method to test rectangular wings in a full-scale, flat-tube heat exchanger. However, they did not test the same heat exchanger geometry without wings. Instead, they compared their measurements to existing correlations. For an isolated tube and multiple rows of wings, they reported a 50% improvement in heat transfer with a 40% pressure drop penalty at $Re = 1000$, based on hydraulic diameter. In 2000, ElSherbini and Jacobi [21] tested delta vortex generators on plain-fin-and-tube heat exchangers. The ratio of wing to heat transfer area was 0.23% and $\alpha = 55°$, $\Lambda = 1$. They achieved a 31% heat transfer enhancement over the baseline, with modest pressure drop penalty of 10% under dry-conditions. Bull and Jacobi [22] reported 10% enhancement in volume goodness factor under dry-conditions for compact plain-fin-and-tube heat exchanger. In this study, $\alpha = 45°$, $\Lambda = 2$ and wing-to-fin area ratio was 0.89%. For wet-conditions the overall enthalpy transfer coeffi-

cient was reduced; however, on the basis of the London area-goodness factor (j/f) the vortex-enhanced surface was found to be comparable to other enhanced surfaces.

Gentry and Jacobi [9] studied the interactions between streamwise vortices induced by a delta-wing vortex generator and the laminar boundary layer on a flat plate. They used quantitative flow visualization and naphthalene sublimation to study flow and heat transfer interactions. Using scaling arguments they asserted that a strong vortex located near the edge of the thermal boundary layer would produce maximum heat transfer enhancement. Then, with a potential flow model of vortex–vortex and vortex–surface interactions, they identified promising generator designs for this simple flat-plate flow. The sublimation data were used to prove the predictive ability of their approach. In an extension to their earlier work, Gentry and Jacobi [12] studied vortices in a developing channel flow and found the vortices spread and traveled away from the winged surface much as in the flat-plate flow near the channel entrance. Once the vortices reached the channel centerline, however, the symmetry in the channel flow caused the vortices to travel in parallel paths down the channel centerline. Vortex circulation was seen to increase with Re_c (based on chord length), Λ, and α. For a particular generator, the dimensionless vortex strength increased by as much as 300% when Re_{dh} increased from 400 to 2000. The vortices had a significant local convective effect on both channel walls, with local enhancements as large as 150% (compared to a channel flow with no vortex generator). Maximum average mass transfer enhancements of approximately 20%, 40%, and 50% were obtained for the entire channel for $Re_{dh} = 400$, 1200, and 2000 respectively. The pressure drop penalty in the channel flow with a vortex generator increased with Re_c, Λ, and α. For $\Lambda = 2.0$ and $\alpha = 55°$, the ratio of the pressure drop with the vortex generator to the pressure drop in the baseline channel flow was approximately 1.5, 1.7, and 2.1 for $Re_{dh} = 400$, 1200, and 2000, respectively.

1.2. Closure

It is established that vortex generation can lead to enhanced heat transfer, and near-optimal generator geometries have been identified for simple flat-plate and channel flows. The enhancement mechanisms are related to enhanced mixing by the swirling motion, boundary-layer thinning by the surface normal secondary flow and flow destabilization (unsteadiness) [3]. Although some work has been reported on full-scale implementation of vortex enhancement in heat exchangers, it appears no work has been reported on vortex enhancement in highly compact heat exchangers that operate under dehumidifying conditions. Such heat exchangers find broad use in systems where space constraints are important (as in automotive systems).

An experimental study to evaluate vortex generation as a heat transfer enhancement for compact heat exchangers operating under both dry- and wet-surface conditions was undertaken. In the remainder of this paper we present a detailed description of the experimental methods, the data reduction and uncertainty, the implementation and evaluation of vortex enhancement, and the thermal-hydraulic performance of a plate-and-fin heat exchanger with and without vortex enhancement.

2. Experimental facility and methods

2.1. Apparatus

A schematic of wind tunnel is shown in Fig. 1. For the current experiments, operating conditions were set to simulate the low-Reynolds-number flows typical to automotive heat exchanger applications. Heaters were installed in two banks: one upstream and one downstream of the axial fan, providing up to 7.5 kW of heat to the air flow. A type-K thermocouple downstream of the main contraction provided feedback to the heater controls. Air temperatures were measured using type-T thermocouples on grids upstream and downstream of the test section. The first grid was located about 200 mm upstream of test specimen; it had six thermocouples evenly spaced in three horizontal zones and two vertical zones. The second grid was located about 225 mm downstream from the specimen, and it had twelve evenly spaced thermocouples in four horizontal and three vertical zones. Each thermocouple was individually referenced to a thermocouple in an ice bath and calibrated to a NIST traceable digital thermometer using a thermostatic bath. The air inlet temperature had an uncertainty of ±0.2 °C. [1] The inlet air temperature profile was flat within ±0.5 °C of the average inlet temperature. The air exit temperature had an uncertainty of ±0.2 °C and was flat within ±1.2 °C of the average exit temperature. Calibration was based on a fifth-order polynomial for each thermocouple. Precautions were taken to keep the wind tunnel free from mass leaks, and the entire duct was wrapped with two layers of 1.27 cm thick foam insulation to mitigate heat losses that might affect temperature measurements.

Chilled mirror hygrometers were used to measure the dewpoint, and they had a measurement uncertainty of ±0.2 °C. Air was supplied to the chilled mirrors through sampling tubes located 30 cm upstream and downstream of the test section. A small, medical diaphragm air pump drew air through sampling tubes. The dewpoint of the incoming air was maintained using a steam injection system. The humidifier could supply up to 11.5 kg/h of

[1] Uncertainties are based on a 95% confidence interval and include all contributions to error.

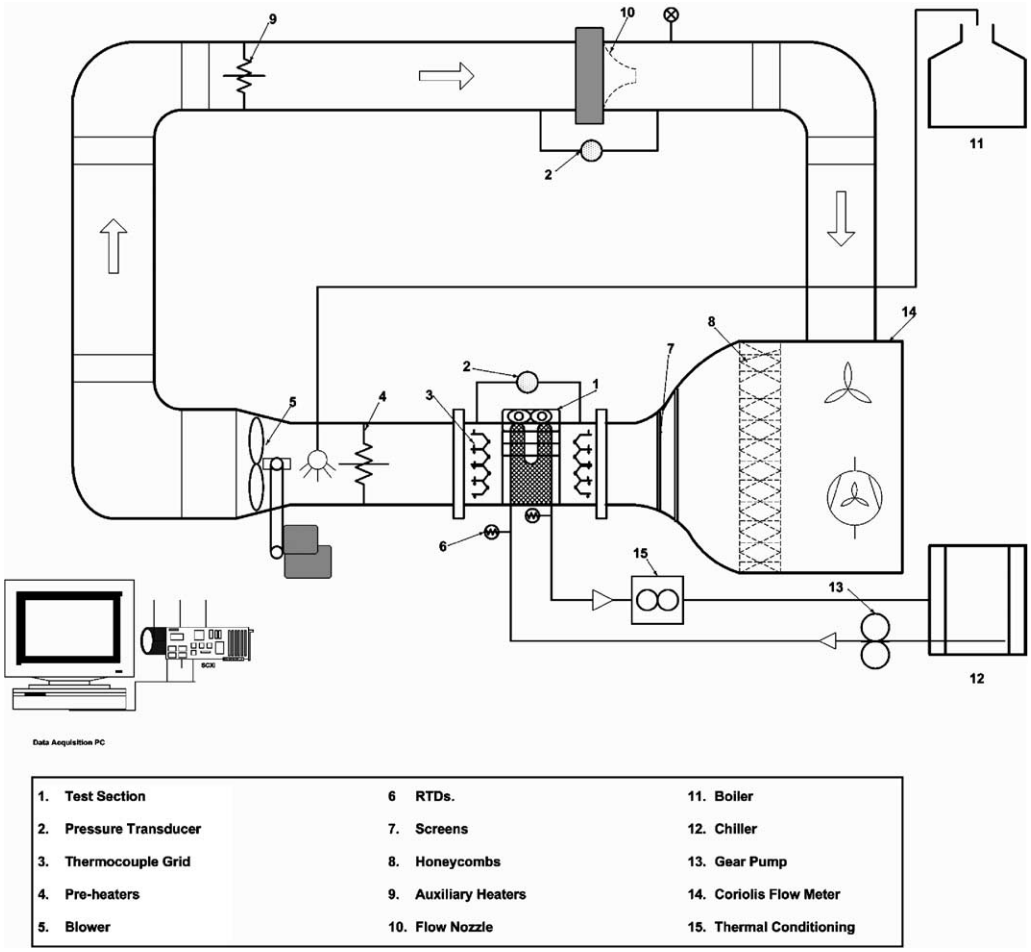

Fig. 1. Schematic diagram of wind-tunnel with descriptors.

steam. The output of the humidifier was controlled by a varying input heater power using a PID controller. The upstream dewpoint monitor provided the control signal for the steam injector. The steam was injected into the tunnel through a perforated pipe 50 cm downstream of first bank of heaters. The axial fan was belt driven by a DC motor and provided a heat exchanger face velocity of up to 4 m/s. Upstream of the test section, air flowed from a thermal mixing chamber and passed through a set of screens, honeycomb flow straighteners, and a 9:1 contraction to obtain steady, laminar flow before passing through the test section. Small, smooth contractions were added up and downstream of the test heat exchanger to provide a perfect match between the heat exchanger face area and the flow cross-section. The test section was carefully insulated to eliminate heat losses between measurement stations. Pressure taps were located on the top and bottom wind-tunnel walls to measure pressure drop across the heat exchanger, approximately 10 cm upstream and downstream of the heat exchanger, with two centered taps at each location spaced 7.5 cm apart. The differential pressure transducers had an uncertainty of ±0.14% of full scale. The air flow rate was measured using an ASME Standard flow nozzle with 152.4 mm throat diameter and diameter ratio of 0.428. The pressure drop across the flow nozzle was measured using a pressure transducer calibrated to an accuracy of ±0.07% of full scale. The absolute pressure at nozzle downstream was measured using an electronic manometer (±0.124 Pa).

A single-phase mixture of ethylene glycol and water was used for the coolant-side flow in the heat exchanger, typically with an ethylene glycol concentration of 35–40% by volume. A NIST traceable hydrometer was used to measure and maintain the specific gravity of the mixture, and mixture properties were obtained by interpolation and curve fits to manufacturer data. Two platinum RTDs were used to measure coolant inlet and outlet temperatures, with a calibration accuracy of ±0.029 C and ±0.022 C for upstream and downstream RTDs, respec-

tively. An R-502 liquid-to-liquid, variable-speed chiller was used to maintain the specified coolant temperature. An immersion temperature probe on the supply line provided the control signal for a proportional controller driving the compressor. The coolant was circulated using a centrifugal pump and a rotary gear pump driven by a 2 HP motor. The coolant flow rate was measured with a Coriolis-effect mass flow meter (±0.5%).

2.2. Procedure

Baseline wind tunnel data were obtained under both dry and wet-conditions without vortex generators. Dry experiments were conducted by setting the inlet coolant temperature to ensure that temperature at the tube wall was everywhere above the dewpoint. Dry conditions were verified by comparing the inlet and outlet dewpoint.

For a typical experiment, the face velocity was set to the desired value along with air and coolant temperatures. The coolant flow rate was fixed to match chiller load. The system was then allowed to run until steady-state conditions prevailed. The system was considered to be at steady state when all temperature fluctuations were less than 0.5 °C for a one-minute period. For a particular experiment, once a steady state was achieved the data were sampled every 2 s and recorded for a period of 300 s. Next, keeping the air-side conditions constant, the coolant flow rate was increased and another data point was obtained. Typically, four or five data-points were obtained for a varying tube-side flow rate and constant air-side conditions. The range of air-side face velocity considered in this work was limited to 1.0–2.0 m/s, because the motivating application (automotive systems) operates in that range. A statistical averaging was performed before data reduction, and an energy balance was calculated to check the veracity of the data.

For wet-surface experiments, steam was introduced into the wind tunnel and the upstream dewpoint was set so that the downstream dewpoint remained above the coolant outlet temperature. This condition is set to ensure fully wet conditions throughout the heat exchanger. The procedure for wet-surface experiments was otherwise identical to those described above for dry-surface experiments.

After obtaining the baseline data under dry and wet conditions, vortex generators were mounted on the leading edges of the fins. Approximately 1500 wings were used in a staggered fashion (see Section 4.1 for details). Thermal-hydraulic experiments were then repeated for the enhanced heat exchanger.

3. Data reduction and interpretation

Data reduction and interpretation follow the methods detailed by the ANSI/ASHRAE Standards (33-2000). The heat exchanger specimen used in this work was a flat-tube (plate) louvered-fin heat exchanger. The geometry of the brazed aluminum exchanger and its partitioning for data reduction are shown in Fig. 2. Each of the two partitions has two coolant passes in cross flow. The coolant enters the inlet manifold and flows through multiple parallel tubes. The number of tubes in each pass was identical. The overall flow arrangement was cross-counter for the first partition and cross-parallel flow for the second partition. The face area was 203 mm × 254 mm. For evaluating thermal performance, the rate equation for the heat exchanger and energy balances between air and coolant sides were employed in conjunction with thermodynamic properties and mass flow rates. An ε–*NTU* method was then used to analyze the heat exchanger performance. The uncertainties in the measurements were propagated to the calculated quantities using the method of Kline and McClintock [23].

3.1. Dry-condition data reduction

From an energy balance on each stream, the following expressions can be written:

$$q_1 = C_{a1}(T_{a,i} - T_{a,o1}), \tag{1}$$

$$q_1 = C_c(T_{c,int} - T_{c,i}), \tag{2}$$

$$q_2 = C_{a2}(T_{a,i} - T_{a,o2}), \tag{3}$$

and

$$q_2 = C_c(T_{c,o} - T_{c,int}), \tag{4}$$

where C_c is the coolant heat rate capacity and C_{a1} and C_{a2} are the air heat rate capacities for the two partitions. The air-side heat capacities are assumed equal for each partition, with their sum equal to C_a. Because, $C_a < C_c$, the heat rates can be expressed in terms of effectiveness as

$$q_1 = \varepsilon_1 C_{a1}(T_{a,i} - T_{c,i}), \tag{5}$$

and

$$q_2 = \varepsilon_2 C_{a2}(T_{a,i} - T_{c,int}). \tag{6}$$

The effectiveness of each of the individual passes in both partitions were considered equal, since the convective heat transfer coefficient was assumed uniform throughout the heat exchanger and the heat capacities were assumed equal. The air flow was unmixed due to the fins, and the coolant side was mixed due to the plate geometry. The effectiveness of a single pass in such a configuration is taken as [24]

$$\varepsilon_p = \frac{\left\{1 - \exp\left[-C_r\left(1 - \exp\left(-\mathrm{NTU}_p\right)\right)\right]\right\}}{C_r}, \tag{7}$$

where C_r is the heat capacity ratio, $C_r = C_{a1}/C_c = C_{a2}/C_c$ The number of transfer units for a single pass is related to the thermal conductance by

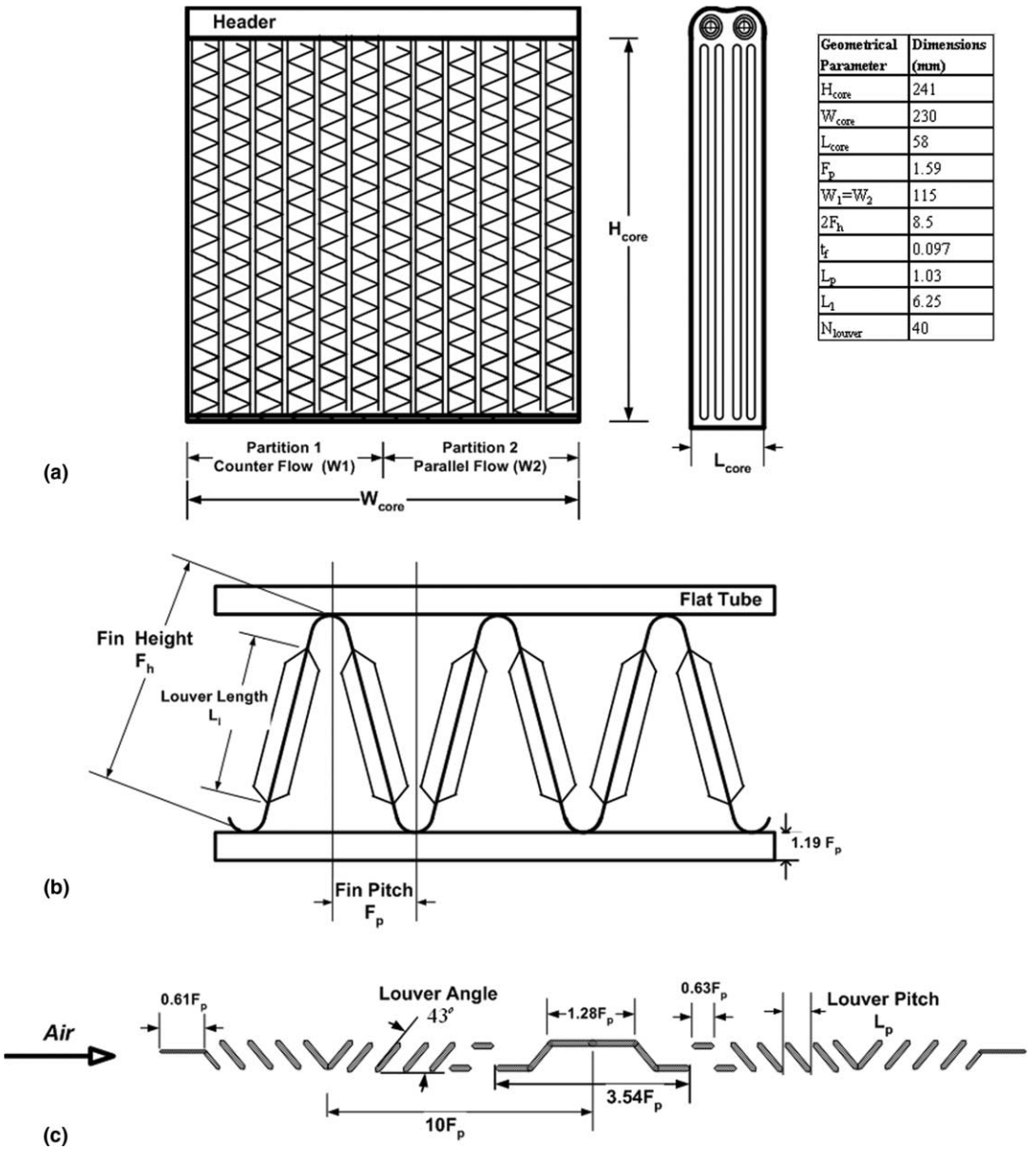

Geometrical Parameter	Dimensions (mm)
H_{core}	241
W_{core}	230
L_{core}	58
F_p	1.59
$W_1=W_2$	115
$2F_h$	8.5
t_f	0.097
L_p	1.03
L_l	6.25
N_{louver}	40

Fig. 2. Schematic diagram of the flat tube louvered compact heat exchanger tested: (a) the frontal and side views showing both partitions, (b) view of fin and louver from air exit side, and (c) Louver fin cross-sectional drawing.

$$\mathrm{NTU_p} = \frac{\mathrm{UA_p}}{C_r}. \tag{8}$$

The effectiveness of the overall counter-flow partition becomes [21]

$$\varepsilon_1 = \frac{\left(\frac{1-\varepsilon_p C_r}{1-\varepsilon_p}\right)^n - 1}{\left(\frac{1-\varepsilon_p C_r}{1-\varepsilon_p}\right)^n - C_r}, \tag{9}$$

where n is the number of passes in the partition. Likewise, the effectiveness of the overall parallel-flow partition is

$$\varepsilon_2 = \frac{1-\left(1-\varepsilon_p(1+C_r)\right)^n}{1+C_r}. \tag{10}$$

In the above equations, the inlet and outlet temperatures, mass flow rates, and specific heat of both the air and coolant are known. The ten equations can be solved simultaneously for the following 10 unknowns: q_1, q_2, $T_{a,o1}$, $T_{a,o2}$, $T_{c,int}$, ε_p, ε_1, ε_2, $\mathrm{NTU_p}$, and $\mathrm{UA_p}$. The overall thermal conductance of the heat exchanger can then be found from

$$\mathrm{UA_T} = 2n\mathrm{UA_p}. \tag{11}$$

The total thermal resistance of the heat exchanger is related to the overall conductance, UA_T, through the following expression:

$$R_T = \frac{1}{UA_T}. \tag{12}$$

Adopting a conventional thermal resistance network for a heat exchanger, the air-side resistance, R_a, is a combination of the resistance due to air-side convection from the tube and the fin (with fin-to-tube contact resistance assumed negligible in this brazed heat exchanger). The total thermal resistance, R_T, is equivalent to the sum of air-side resistance, tube conduction resistance, and tube-side convection resistance; therefore, using Eq. (12).

$$\frac{1}{UA_T} = (R_w + R_a) + \frac{D_{tube}}{k_c Nu_c A_{tube}} \tag{13}$$

In Eq. (13), it is clear the tube-side resistance is inversely proportional to the Nusselt number, Nu_c which is calculated based on hydraulic diameter of the tube. The correlation by Emerson [25] for a flat-plate tube was used to model the tube-side Nusselt number, since it is believed to be most appropriate for the Reynolds number range under consideration ($1 < Re_c < 1000$), namely

$$Nu_c = 0.625 Re_c^{0.34} Pr_c^{0.33} \left(\frac{\mu_w}{\mu_c}\right)^{-0.14}. \tag{14}$$

During the data reduction, the tube wall resistance was found to be about 0.1% of the total thermal resistance, and it was therefore neglected.

The air-side resistance, R_a, is found by subtracting the tube-side resistance from the total resistance, R_T. The air-side convection coefficient is calculated using the following relation:

$$R_a = \frac{1}{\eta_o h A_T}, \tag{15}$$

where A_T is the total surface area associated with both the fins and the exposed portion of the base, h is air-side heat transfer coefficient and η_o is the overall surface efficiency which is defined as

$$\eta_o = 1 - \frac{NA_f}{A_T}(1 - \eta_f), \tag{16}$$

where N is number of fins in the test section, A_f is surface area of each fin and η_f is the individual fin efficiency. For fin efficiency calculation, the fin geometry was modeled as a straight fin with an adiabatic tip (along the line of symmetry between tubes). Since each fin is symmetrically placed between the tubes, the geometric centerline is taken as adiabatic. Fin efficiency for the dry surface is written as [25]

$$\eta_f = \frac{\tanh(m_d L_f)}{m_d L_f} \tag{17}$$

where

$$m_d = \sqrt{\frac{2h}{k_f t_f}} \tag{18}$$

taking into account the fact that the fin width is much greater than its thickness. Eqs. (15), (17) and (18) are solved iteratively to obtain the convection coefficient, h.

The friction factor is expressed as

$$f = \frac{2\Delta P_{core}\rho_{ma}}{G^2}\left(\frac{A_{min}}{A_T}\right) - (1+\sigma^2)\left(\frac{\rho_{a,i}}{\rho_{a,o}} - 1\right)\left(\frac{A_{min}}{A_T}\right)\left(\frac{\rho_{a,i}}{\rho_{a,o}}\right) \tag{19}$$

where $\rho_{a,i}$ and $\rho_{a,o}$ are the density of air at the inlet and outlet of the heat exchanger. The Colburn *j-factor* is expressed as

$$j = St\,Pr^{2/3}, \tag{20}$$

where

$$St = \frac{h}{G c_{p,ma}}, \tag{21}$$

with G the mass velocity, ρV_{max} and $c_{p,ma}$ the mean specific heat of air. The maximum air velocity, V_{max}, corresponds to the minimum free flow area, A_{min}. The air-side Reynolds number Re_a is based on hydraulic diameter and the mass velocity. The volume goodness factor comparison is defined as below:

$$Z = \eta_o h \beta, \tag{22}$$

$$E = \Delta P_{core}\left(\frac{\dot{m}_a}{A_T \rho_{ma}}\right)\beta \tag{23}$$

where Z represents the heat transfer per unit temperature difference and per unit core volume. E represents the fan power per unit core volume and β is the total heat transfer surface area per unit core volume.

3.2. Wet-condition data reduction

Under de-humidifying conditions, the calculation procedure is modified by latent heat transfer and the presence of a water film on the air-side surface. The overall data reduction procedure follows the same methodology as in dry conditions. The energy balance on air stream for first partition is written as

$$q_1 = \dot{m}_{a1}(i_{a,i} - i_{a,o1}), \tag{24}$$

where $i_{a,i}$ and $i_{a,o}$ are inlet and outlet enthalpies of moist air. An analogous relation applies for second partition. The heat exchanger rate equation, based on enthalpy potential, can be expressed as

$$q_1 = \varepsilon_1 \dot{m}_{a1}(i_{a,i} - i_{a,min\,1}), \tag{25}$$

where, $i_{a,min1}$ is the enthalpy of moist air at fin surface temperature corresponding to refrigerant inlet tem-

perature and 100% relative humidity. The fin surface temperature is estimated by subtracting the coolant-side convective resistance while neglecting conduction resistance as follows:

$$T_{a,s1} = T_{c,i} + \frac{q_m}{h_c A_c}. \tag{26}$$

Similar relations apply for the second partition.

Eqs. (1), (3), (5) and (6) are replaced with relations typical to (24) and (25) for the respective partitions, in order to compute the overall conductance UA_T. The tube-side thermal resistance is then subtracted from R_T to isolate the air-side resistance. However, the fin efficiency under de-humidifying conditions is calculated using the method presented by Wu and Bong [26]. They assumed a linear relationship between ω_s, the humidity ratio of the saturated air at the wet surface, and T_f, the fin surface temperature. This assumption allows analytical solution of fin equation when Colburn–Chilton heat mass analogy holds:

$$\eta_f = \frac{\tanh(mL_f)}{mL_f}, \tag{27}$$

where m is related to m_d in the dry fin efficiency expression by

$$m^2 = m_d^2(1 + b_s\xi) \tag{28}$$

with

$$\xi = \frac{i_{vap}}{c_p L e^{1/3}}, \tag{29}$$

and b is the average slope of the saturation line from $T_b < T_f < T_t$, written as

$$b_s = \frac{(\omega_{s,t} - \omega_{s,b})}{T_t - T_b}, \tag{30}$$

where the subscripts b and t refer to fin base and geometric center respectively. With the fin efficiency known, the overall surface effectiveness in wet-conditions is again calculated using Eq. (16).

4. Results

4.1. Vortex generator geometry

In a conventional water tunnel, using simple dye-and-water visualization, a visual study of vortex generation was used to establish a wing design for this heat exchanger. Flow visualization allowed a quick but qualitative evaluation of vortex coherence and longevity for a range of candidate winglets. Because of space limitations, this preliminary visualization work is not described in detail here, but the resulting generator geometry will be described in detail.

The best results were obtained for winglets with $b = 2F_p$, $\Lambda = 0.8$, and $\alpha = 45°$. The wing centerline was offset from the fin base by 1/4 of its span. For this design, the vortices were seen to be well defined and coherent. They entered the fin space cleanly and survived about 70% of the flow length. The most important parameters influencing the performance of the vortex generators were identified to be angle of attack and aspect ratio. At higher angles of attack (~55°), early vortex breakdown was observed and at low angles (~25°), the vortices had poor stability and did not enter the fin spaces cleanly. Similarly the parametric study revealed that at higher aspect ratios (~10), the vortices were of low strength compared to lower aspect ratios. However, at lower aspect ratios (e.g., ~1.8), the vortices were unstable and did not make a clean entry into the adjacent fin spaces.

Due to the fin geometry and orientation, in order to introduce one vortex between each pair of fins it was necessary to use a staggered arrangement of wings on either side of fin column as shown schematically in Fig. 3(a). In order to facilitate accurate wing mounting, multiple wings were mounted on an EDM-manufactured strip as shown schematically in Fig. 3(b). Two such strips of 32 wings were used on each of the 24 fin columns consisting of 128 fins per column. The original length of the strip was identical to the tube height of the heat exchanger and segments of strips were then aligned and glued on the flat-plate-tubes at the leading edge of the fin. The final implementation of vortex generators on the heat exchanger is also shown in the photograph at Fig. 3(c).

4.2. Dry-surface experiments

The energy balances between air and coolant sides were used to ascertain the performance of the test apparatus. For 90% of the data, the energy transfer rates were within 5% of each other. The energy balance criterion used here was based on the deviation from mean heat transfer rate. The dry-surface thermal performance of the heat exchanger after attaching the delta-wing vortex generators is compared to its original performance without the generators in Fig. 4, where the heat transfer coefficient and air-side thermal resistance are presented. Over the range of face velocities considered in this study, the vortex generators caused an average increase of 21% in the heat transfer coefficient. Using a 95% confidence interval and standard error-propagation analysis, the relative uncertainly in air-side convection coefficient was estimated to be less than 8%, demonstrating a significant enhancement. The air-side resistance is also seen to drop by approximately the same magnitude. The heat transfer results were also calculated in terms of Colburn j-factors, which are enhanced (with differences due to experimental uncertainties).

It may be noted that the wings were mounted on tube edge using low-conductivity glue. Hence, the wings did

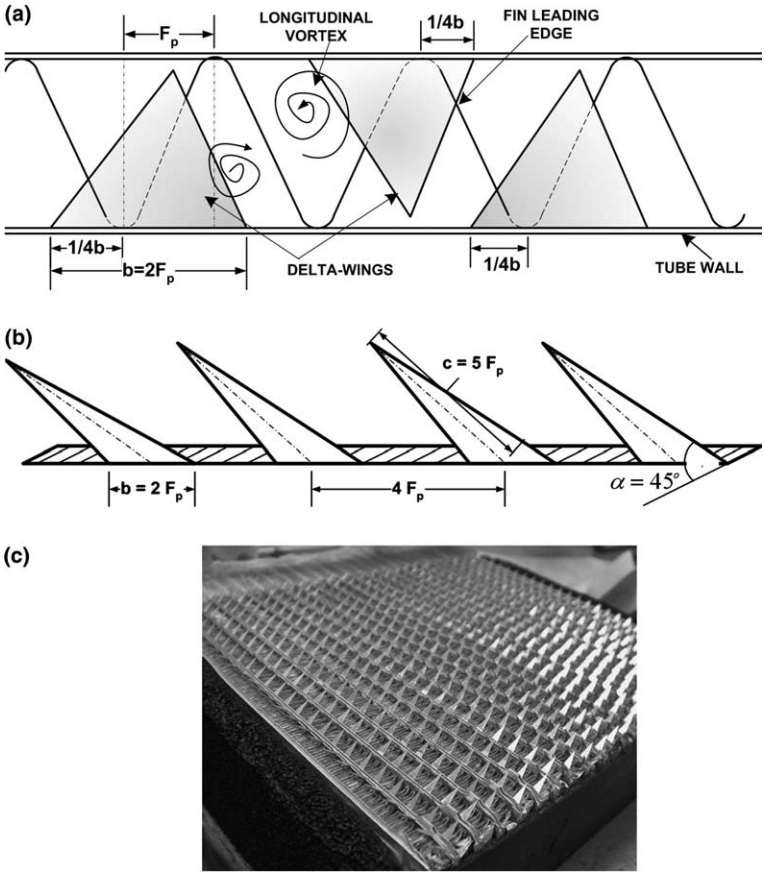

Fig. 3. Vortex generator implementation: (a) wing placement as shown (with a 1/4-span offset) ensures provides one vortex passes into each inter-fin space; (b) wings are manufactured by wire EDM as strips with 10–20 wings each; (c) fixing the strips to the face of the heat exchanger provides approximately 1500 delta-wing vortex generators in a staggered pattern.

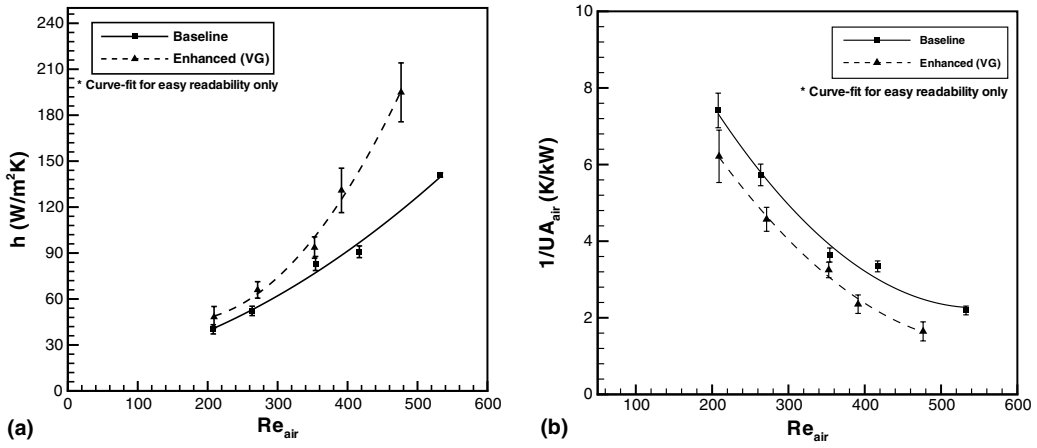

Fig. 4. Baseline and enhanced thermal performance under dry-surface conditions: (a) heat transfer coefficient versus Reynolds number; (b) thermal resistance is plotted against air-side Reynolds number. In either representation, the enhancement is clearly larger than the experimental uncertainty.

not increase the effective heat transfer area of the either fin or tube, and the overall decrease in air-side resistance can be attributed to the generated vortices. The wing-to-fin area ratio was 0.48%. It is pertinent to mention that

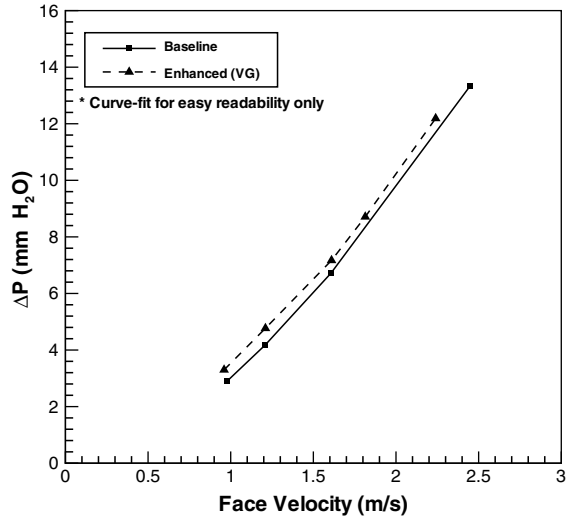

Fig. 5. Baseline and enhanced hydraulic performance under dry-surface conditions. Pressure drop across the heat exchanger is plotted as a function of face velocity.

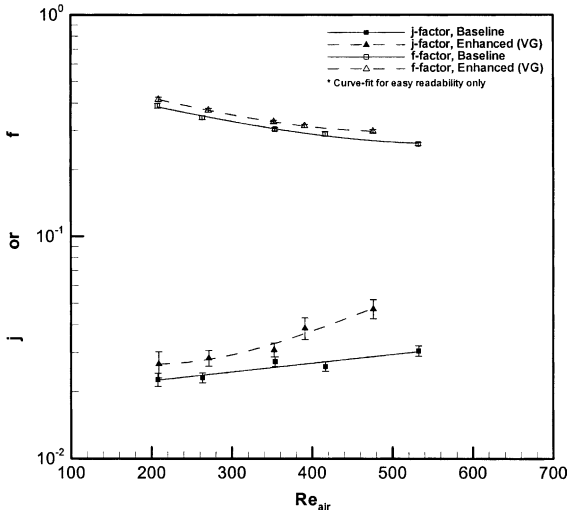

Fig. 6. The conventional representation of thermal and hydraulic performance under dry-surface conditions is shown, with the Colburn *j*-factor and friction factor plotted against Reynolds number for the baseline and enhanced heat exchanger. The average increase in *j*-factor was 28% with modest pressure drop penalty of 6.6%.

an optimal wing geometry and placement was not achieved the design was considered 'workable', and further research on vortex generation might lead to a larger heat transfer enhancement.

The pressure drop data are presented in Fig. 5, which shows the actual pressure drop across the heat exchanger before and after mounting vortex generators at different face velocities. The pressure drop increases monotonically with face velocity in both the cases. The figure indicates that the delta-wings did not cause a significant change in pressure drop. The corresponding non-dimensional friction factor data are presented in Fig. 6 along with the Colburn *j-factor*, which is plotted against air-side Reynolds number. As the air Reynolds number is increased, the friction factor decreases gradually in a non-linear fashion, as is typical to this class and type of heat exchanger. The average decrease in friction factor over the range of Reynolds number considered was found to increase 6.6% with the addition of the vortex generators; the uncertainty in friction factor is about 6%.

It is common for heat transfer enhancement techniques to be accompanied by a pressure drop penalty. Previous investigations of channel flows have shown that enhancements by way of vortex generators are associated with pressure drop penalty of same order as that of heat transfer enhancement. The low pressure drop penalty incurred with this geometry opens new possibilities. Multiple rows of vortex generators can be considered for further enhancing heat transfer performance. It is expected that the use of multiple rows of generators would increase the pressure drop, but the heat transfer enhancement might offset the pressure drop penalty to give an overall increase in performance. In any case, the important point is that the pressure drop does not limit implementation of this method in this highly compact heat exchanger geometry.

The overall performance of the delta-wing vortex generator is evaluated using the criterion of London area-goodness factor, *j/f*, and also the volume goodness factor. The baseline (un-enhanced) results are compared to the enhanced performance in Fig. 7. For the Reynolds number range pertinent to the heat exchanger under consideration, the delta-wings improved the *j/f* ratio 19% over the baseline case, with similar enhancements reflected by volume goodness. All the heat transfer performance curves, including '*h*' and '*f*', show a distinctive trend of low enhancement at lower Reynolds numbers and a non-linear increase at progressively higher Reynolds number flows. There could be two explanations for this behavior. Firstly, the strengths of the vortices generated at low air velocities are expected to be weaker than at higher velocities, resulting in less impact. Secondly, there is a flow transition from louvered-directed to duct-directed flow at low air-side Reynolds numbers [27]; thus, the *j-factor* decreases at low Reynolds numbers, without a commensurate decrease in the friction factor. It should also be noted that experimental uncertainty is highest at low air-side flow rates.

4.3. Wet-surface experiments

The energy balances between air and coolant sides were within 5% of each other for 88% of the data. The performance evaluation criteria employed under fully wet-conditions are similar to those used for dry-condi-

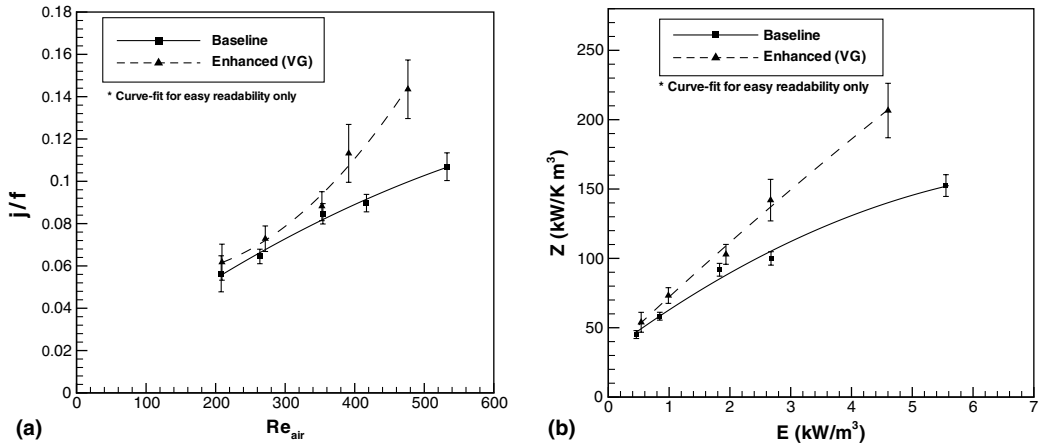

Fig. 7. Conventional heat-exchanger performance evaluation criteria are applied to assess the impact of vortex enhancement on the thermal-hydraulic performance under dry-surface operating conditions: (a) the area goodness factors, *j/f*, for the baseline and enhanced heat exchangers; and (b) the volume goodness factor, *Z*, for the baseline and enhanced heat exchangers.

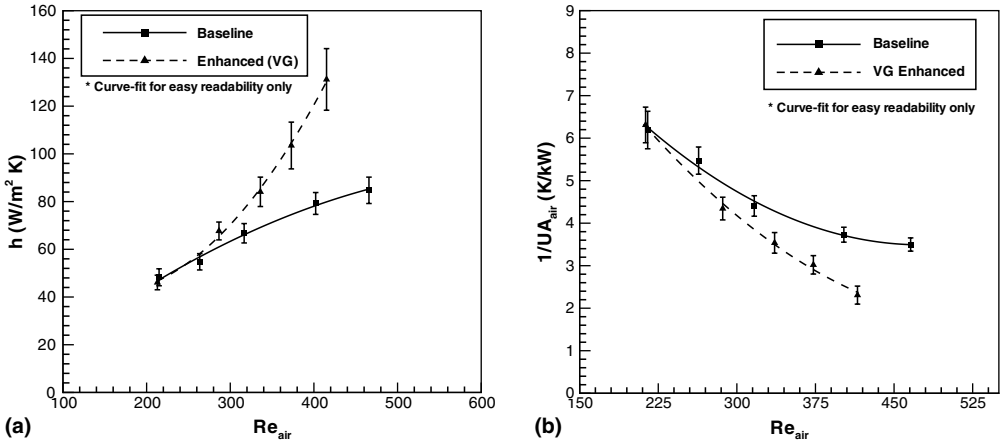

Fig. 8. Baseline and enhanced thermal performance under wet-surface conditions: (a) heat transfer coefficient versus Reynolds number; (b) thermal resistance is plotted against air-side Reynolds number. In either representation, the enhancement is clearly larger than the experimental uncertainty.

tions; however, under de-humidifying conditions the overall heat transfer rate includes the effects of both sensible and latent heat transfer. The results of vortex enhancement, in terms of air-side thermal resistance and heat transfer coefficient, are shown in Fig. 8. The air-side thermal resistance decreased for the vortex-enhanced case; however, the behavior is more complex than for the dry-surface case.

At air-side Reynolds numbers below about 300, no significant enhancement in heat transfer coefficient is observed. At low air velocities, shear and pressure forces are small in comparison to gravitational forces on condensate droplets. Under these conditions, more condensate is retained on the air-side surface, and this retained water might reduce the impact of vortex generation. On an average basis over the face velocity range considered here, the heat transfer coefficient for the delta-wing enhanced surface was 23.4% higher than for the baseline surface, well above the data uncertainty of about 8%. The enhancement in this case is about same order as that achieved for the dry-conditions.

The pressure drop measurements are shown in Fig. 9 for the heat exchanger before and after mounting the vortex generators. The pressure drop increases monotonically with air mass flow rate for both cases under wet conditions. As expected, the pressure drop is higher than for the dry conditions. The retained condensate introduces a "flow blockage" effect resulting in higher friction and pressure drop.

Fig. 10 shows the *j* and *f* data as a function of air-side Reynolds number. The *j-factor* increased by 25.2% and *f-factor* by 6.6%. These results indicate that the vortex

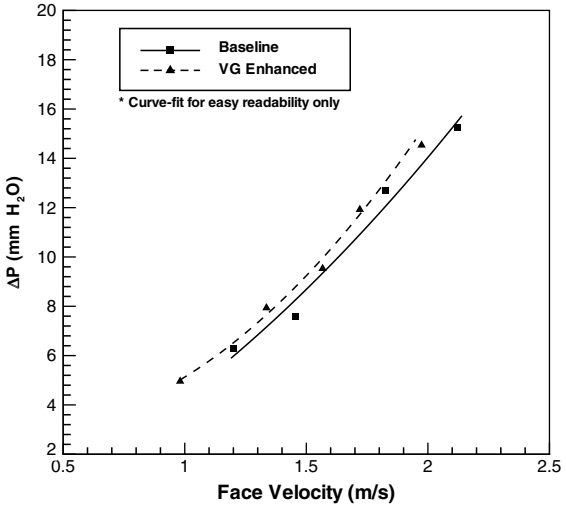

Fig. 9. Baseline and enhanced hydraulic performance under wet-surface conditions. Pressure drop across the heat exchanger is plotted as a function of face velocity.

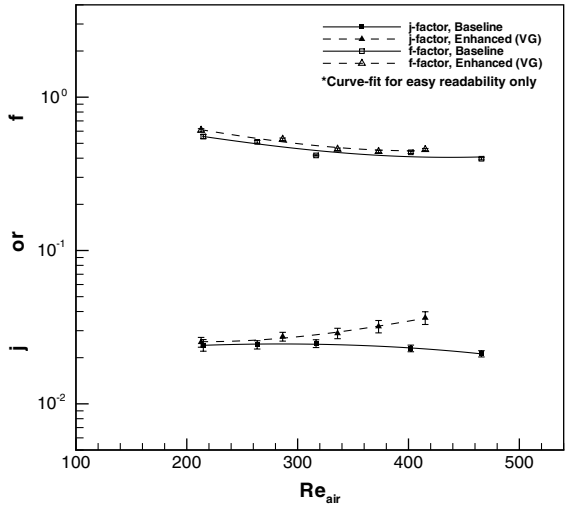

Fig. 10. The conventional representation of thermal and hydraulic performance under wet-surface conditions is shown, with the Colburn *j*-factor and friction factor plotted against Reynolds number for the baseline and enhanced heat exchanger. The *j*-factor increased by 16.6% and *f*-factor increased by 6.6%.

generators did not cause any significant pressure drop penalty as was the case for dry results. The overall performance of the delta-wing vortex generator is evaluated using London area-goodness factor, *j*/*f*, and compared to baseline performance in Fig. 11. The wings improved the performance by an average 22.7% over the parameter range of these experiments.

5. Conclusions and future work

Contemporary louvered-fin heat exchangers have been heuristically optimized by industry and are reaching their performance limits. In order to assess an emerging enhancement that might meet the next-generation performance needs of compact heat exchangers, the effectiveness of delta-wing type vortex generators is evaluated in this work. Guided by past research and an understanding of the mechanisms of vortex generation, a working design for delta-wing type vortex generators was developed using flow visualization for a plain-channel geometry. This approach and design are considered adequate for the current purpose of proved viability, future efforts toward optimal design should consider flow visualization in louvered-fin geometry.

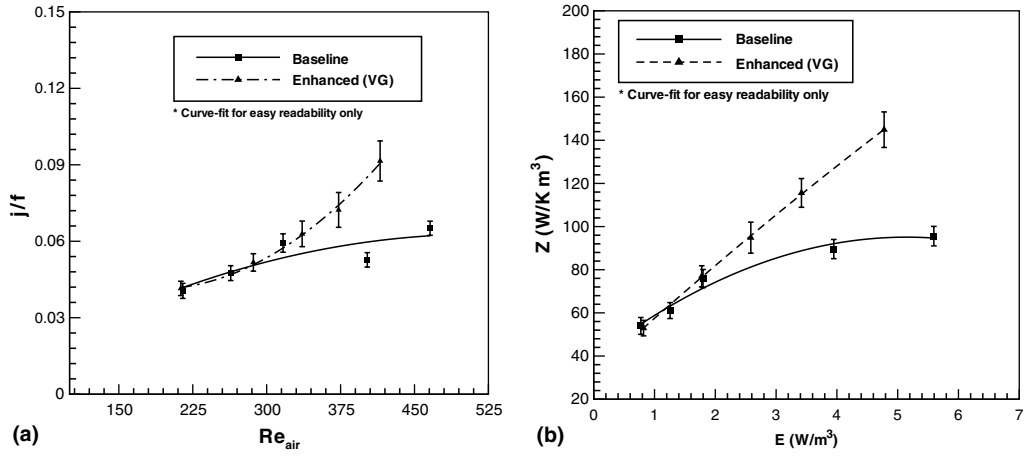

Fig. 11. Conventional heat-exchanger performance evaluation criteria are applied to assess the impact of vortex enhancement on the thermal-hydraulic performance under wet-surface operating conditions: (a) the area goodness factors, *j*/*f*, for the baseline and enhanced heat exchangers; and (b) the volume goodness factor, *Z*, for the baseline and enhanced heat exchangers.

The baseline heat transfer and pressure drop performance of a louvered-fin heat exchanger were obtained in full-scale calorimetric wind-tunnel experiments and compared to the performance obtained after mounting approximately 1500 delta wings on the heat exchanger face. The results have demonstrated a favorable impact of delta-wings on the performance of a compact heat exchanger used in automotive applications. Average heat transfer enhancements of 21% over baseline conditions were achieved under dry conditions, and enhancements of 23.4% over baseline conditions were achieved for wet-surface conditions. The pressure drop penalty associated with these heat transfer enhancements was about 6%. It is believed that this first-cut design can be further improved by optimization with respect to both wing geometry and placement. For example, employing an array of VGs along the flow path instead of just one at leading edge might significantly improve performance.

Although it is clear that condensate retention plays a role in vortex enhancement, the relationships between vortex flow, retained condensate, heat transfer enhancement, and sensible heat ratio are not very well understood. Further work in this area is needed.

References

[1] A.M. Jacobi, R.K. Shah, Heat transfer surface enhancement through the use of longitudinal vortices: a review of recent progress, Exp. Thermal Fluid Sci. 11 (1995) 295–309.

[2] M. Fiebig, Vortex generators for compact heat exchangers, J. Enhanced Heat Transfer 2 (1–2) (1995) 43–61.

[3] M. Fiebig, Vortices, generators and heat transfer, Chem. Eng. Res. Design 76 (A2) (1998) 108–123.

[4] G. Biswas, K. Torii, D. Fujii, K. Nishino, Numerical and experimental determination of flow structure and heat transfer effects of longitudinal vortices in a channel flow, Int. J. Heat Mass Transfer 39 (4) (1996) 3441–3451.

[5] F. Dupont, C. Gabillet, P. Bot, Experimental study of the flow in compact heat exchanger channel with embossed-type vortex generators, J. Fluids Eng. 125 (2003) 701–709.

[6] F.J. Edwards, C.J.R. Alker, The improvement of forced convection surface heat transfer using surface protrusions in the form of (A) cubes and (B) vortex generators, Proc. 5th Int. Heat Transfer Conf. 2 (1974) 244–248.

[7] K. Katoaka, H. Doi, T. Komai, Heat/mass transfer in Taylor vortex flow with constant axial flow rates, Int. J. Heat Mass Transfer 20 (1977) 57–63.

[8] K. Torii, J.I. Yanagihara, Y. Nagai, Heat transfer enhancement by vortex generators, Proc. ASME/JSME Thermal Eng. Joint Conf. 3 (1991) 77–83.

[9] M.C. Gentry, A.M. Jacobi, Heat transfer enhancement by delta-wing vortex generators on a flat plate: vortex interactions with the boundary layer, Exp. Thermal Fluid Sci. 14 (3) (1997) 231–242.

[10] J.I. Yanagihara, K. Torii, Heat transfer augmentation by longitudinal vortices, Proc. 3rd World Conf. Exp. Heat Transfer, Fluid Mech. Thermodynamics 1 (1993) 560–567.

[11] M. Fiebig, P. Kallweit, N.K. Mitra, Wing type vortex generators for heat transfer enhancement, Proc. 8th Int. Heat Transfer Conf. 6 (1986) 2909–2913.

[12] M.C. Gentry, A.M. Jacobi, Heat transfer enhancement by delta-wing-generated tip vortices in flat-plate and developing channel flows, J. Heat Transfer 124 (2002) 1158–1168.

[13] H. Ge, A.M. Jacobi, J.C. Dutton, Air-side heat transfer enhancement in offset-strip fin array using delta-wing vortex generators, air conditioning and refrigeration center, ACRC Report TR-205, University of Illinois, Urbana, 2002.

[14] G. Biswas, H. Chattopadhyay, Heat transfer in a channel with built-in wing-type vortex generators, Int. J. Heat Mass Transfer 35 (4) (1992) 803–814.

[15] M. Brockmeier, T. Guntermann, U. Fiebig, Performance evaluation of a vortex generator heat transfer surface and comparision with different high performance, Int. J. Heat Mass Transfer 36 (10) (1993) 2575–2587.

[16] M. Fiebig, A. Valencia, N.K. Mitra, Wing-type vortex generators for fin-and-tube exchangers, Exp. Thermal Fluid Sci. 7 (4) (1993) 287–295.

[17] G. Biswas, N.K. Mitra, M. Fiebig, Heat transfer enhancement in fin-tube heat exchangers by winglet type vortex generators, Int. J. Heat Mass Transfer 37 (2) (1994) 283–291.

[18] M. Fiebig, Y. Chen, A. Grosse-Gorgemann, N.K. Mitra, Conjugate heat transfer of a finned tube Part B: heat transfer augmentation and avoidance of heat transfer reversal by longitudinal vortex generators, Numer. Heat Transfer A: Appl. 28 (2) (1995) 147–155.

[19] A. Jahromi, A. Bastani, N.K. Mitra, G. Biswas, Numerical investigations on heat transfer in a compact fin-and-tube heat exchanger using delta winglet type vortex generators, J. Enhanced Heat Transfer 6 (1) (1999) 1–11.

[20] C.M.B. Russell, T.V. Jones, G.H. Lee, Heat transfer enhancement using vortex generators, Proc. 7th Int. Heat Transfer Conf. 3 (1982) 283–288.

[21] A. ElSherbini, A.M. Jacobi, The thermal-hydraulic impact of delta-wing vortex generators on the performance of a plain-fin-and-tube heat exchanger, J. HVAC&R Res. 8 (2002) 357–370.

[22] B.R. Bull, A.M. Jacobi, A study of the application of vortex generators to enhance the air-side performance of heat exchangers, air conditioning and refrigeration center, ACRC Report TR-214, University of Illinois, Urbana, 2003.

[23] S.J. Kline, F.A. McClintock, Describing uncertainties in single sample experiments, Mech. Eng. 75 (1953) 3–8.

[24] F.P. Incropera, D.P. DeWitt, Fundamentals of Heat and Mass Transfer, fifth ed., John Wiley, New York, 2002.

[25] A.C. Talik, L.W. Swanson, L.S. Fletcher, N.K. Anand, Heat transfer and pressure drop characteristics of a plate heat exchanger, Proc. ASME/JSME Thermal Eng. Joint Conf. 4 (1995) 321–329.

[26] G. Wu, T.P. Bong, Overall efficiency of a straight fin with combined heat and mass transfer, ASHRAE Trans. 100 (1994) 367–374.

[27] A. Achachia, T.A. Cowell, Heat transfer and pressure drop characteristics of flat plate tube louvered heat exchanger, Exp. Thermal Fluid Sci. 1 (1988) 147–157.